

Hyperfine fields and local-moment formation at 3*d*-series impurities in terbium

J. Boysen, J. Grimm, A. Kettschau,* and W. D. Brewer

Fachbereich Physik, Freie Universitaet Berlin, D-1000 Berlin 33, Germany

G. V. H. Wilson

*Department of Physics, University College, The University of New South Wales, Campbell,
Australian Capital Territory, Australia 2600*

(Received 21 July 1986)

We report the observation of low-temperature nuclear orientation of radioactive Sc, V, Cr, Mn, and Co as extremely dilute impurities in ferromagnetic terbium. A model based on the crystalline anisotropy of Tb and supported by measurements on ^{160}Tb in the same samples was used to extract the hyperfine fields at the 3*d* impurity sites. Together with the previously known field at FeTb, this essentially completes the systematics for first transition-series impurities in this host; our values for B_{hf} are for ScTb, $-2.0(4)$ T; VTb, $-2.4(5)$ T; CrTb, $+11.6(1.0)$ T; MnTb, $+20.0(1.0)$ T; and CoTb, $-2.0(3)$ T. We discuss the decomposition of these fields into local and transferred contributions and the derivation of local moments from the former.

I. INTRODUCTION

The systematics of hyperfine interactions (HFI's) at dilute impurities in metals can give information about the electronic structure of the host, as well as about the formation (or retention) of local moments on the impurity ions and their interaction with the host electrons.¹⁻⁴ In the case of impurities from the first (and second) transition series, orbital angular momentum on the impurity is usually considered to be quenched, and, due to the generally small nuclear quadrupole moments and antishielding factors, the HFI is purely magnetic, consisting of hyperfine-field contributions from the host (transferred hyperfine interaction and host conduction-electron polarization in the case of an ordered host material) and from the impurity ion itself (local contribution).⁵⁻⁷

For the 3*d* ferromagnetic hosts Fe and Ni, such HFI data have been available for over 25 years, from nuclear specific heats,⁸ NMR,^{9,10} and excited-nucleus methods [Mössbauer effect (ME), perturbed angular correlations (PAC), and low-temperature nuclear orientation¹¹⁻¹³ (NO)]. Additional insight into the formation of local moments has been obtained from concentration-dependent magnetic measurements¹⁴ and neutron scattering.^{15,16} In contrast, the data for Co and for Gd, whose *S*-state ions make it in many respects similar to the 3*d* elemental ferromagnets, are more sparse,¹⁷ although the general trends are clear. In the other heavy rare earths (RE), where large orbital moments are accompanied by strong crystalline anisotropies and complex magnetic structures, very few data on the HFI of transition-element impurities have been available. This is due in part to the very low solubilities and the tendency to compound formation in these alloy systems, which necessitate the use of extremely dilute samples and preclude many of the experiments mentioned above. Furthermore, the large magnetic anisotropies of these hosts make polycrystalline samples impossible to magnetize with available fields and thus often necessitate

the use of single crystals, making sample preparation expensive and complex; or else they depend on a model to allow the interpretation of data from magnetically unsaturated samples. With the latter approach, the HFI's at several impurities from the 5*d* series in Dy and Tb were studied by PAC some years ago.¹⁸ Here, we report results of a similar study of impurities from the first transition series (Sc, V, Cr, Mn, and Co) by NO, which, combined with a result for Fe from the literature,¹⁹ completes the systematics for Tb and complements the investigation begun in the 1970s on the Gd host.²⁰⁻²² As a basis for the interpretation of these experiments, the HFI of Tb in Tb single crystals has been studied in preliminary work.²³⁻²⁵ The present results, examined by means of a decomposition of the magnetic hyperfine fields, give the first information on the presence of local moments on transition impurities in Tb and permit a comparison with Gd host, with its much simpler magnetic structure.

The spirit of this work is much the same as that of Ref. 21, where very dilute samples of 3*d* and 4*d* elements in Gd were investigated by NO. The resulting hyperfine-field systematics were compared to those in Ni, showing that Gd has considerable similarity to a *d*-band ferromagnet and represents a mirror image of Ni in its behavior with regard to the formation of local moments on impurities. The extreme sensitivity of NO permits the use of impurity concentrations below 1 ppm, and rapid cooling of these dilute samples from near the melting point avoids precipitation or compound formation of the impurities. Simultaneous study of the HFI of impurity nuclei and of ^{160}Tb nuclei in the same sample permits the direct determination of the quantization-axis distribution due to incomplete magnetic saturation, and thus allows the evaluation of the magnetic hyperfine fields acting on the impurity nuclei at $T=0$. Preliminary results for Cr and Mn impurities have been reported by Grimm *et al.*^{23,26}

In Sec. II we describe experimental procedures and sample preparation. Section III summarizes the data analysis, particularly the assumptions used to extract HFI

information from data on incompletely-saturated samples. Section IV discusses the results and the derivation of local moments, comparing them with data obtained for other ferromagnetic host metals. Our conclusions are briefly summarized in Sec. V.

II. EXPERIMENTAL PROCEDURES

A. Sample preparation

Due to the above-mentioned problems of limited solubility and tendency to compound formation, as well as the considerable chemical reactivity of the rare-earth host-metal terbium, the dilute transition-metal alloys used in this work were prepared by rapid quenching of molten ingots in an inert atmosphere. The starting materials were 3*N* plus polycrystalline Tb (Ref. 27) and trace amounts (typically 30 μ Ci) of radioisotopes obtained from commercial suppliers as dilute chloride solutions. All of the isotopes used were carrier free except ^{60}Co , which contains about a tenfold concentration of stable ^{59}Co due to the reactor irradiation. Wedge-shaped pieces of Tb were cut from the ingot as received and drilled to form small crucibles weighing about 600 mg. An appropriate amount of methanolic radioisotope solution was dropped into the well in each crucible and evaporated to dryness. The crucibles were then placed on a water-cooled Cu cold finger in high-purity argon atmosphere (repeated pumping with cryosorption pumps and flushing with purified Ar), together with a piece of Gd or Tb getter material. Using an induction furnace, the getter was first melted, further purifying the Ar atmosphere; then each Tb sample was melted and maintained for about a minute in the molten state, giving complete reduction of the transition-metal trace impurities and good mixing due to the stirring action of eddy currents in the molten samples. The induction furnace also produces a partial levitation of the samples above the cold Cu hearth, reducing thermal contact to the latter. Sudden removal of power causes the sample to drop onto the hearth and chill rapidly to near room temperature. The resulting ingots were nearly spherical and had a metallic sheen. In most cases, they were pressed mechanically between Ta foils to give disks of about 10 mm diameter and 1 mm thickness, which were then irradiated with thermal neutrons in the BER-II reactor to produce an additional 10 μ Ci of ^{160}Tb activity. Some samples were studied in the spherical form, and some were annealed in pure Ar at 850°C for 24 h to investigate the effect of defects produced by the mechanical treatment or the irradiation. Pieces of appropriate size, usually about $\frac{1}{4}$ of the disk, were cut and mounted in the NO cryostat as described below. The added impurity concentration was in all cases below 1 ppm, in most cases less than 10 ppb. Standard nuclear orientation thermometers ($^{57,60}\text{CoFe}$, $^{57,60}\text{CoNi}$, $^{54}\text{MnNi}$) were used in appropriate combinations on the sample holder and the sample itself to determine its temperature.

B. Cryogenics

Good thermal contact to the samples is essential in these experiments, not only because of the need for accu-

rate thermometry but also because of radioactive heating (due to absorption of radiations in the thick samples) and the samples' large nuclear Schottky heat capacities. In fact, in the first reported NO experiment on Tb metal,²⁸ no γ -ray anisotropy was seen, probably due to poor thermal contact to the samples and resulting failure to cool through the Schottky peak near 160 mK. In the present case, both sides of the disks were tinned with pure In using a commercial ultrasonic soldering iron, after surface cleaning with fine emery paper. Care was taken to maintain the soldering temperature near the indium melting point. Excellent tinning was obtained in this way without a protective atmosphere, in contrast to results reported for some other rare-earth samples.²⁹ (In fact, in one experiment in which the Tb sample was accidentally mounted off center in the 7-T polarizing coil, the 1-mm-thick copper sample holder was bent double by magnetic forces on the Tb without noticeable failure of the solder joint.) In initial experiments, NO thermometers were attached both to the back of the sample holder and to the free face of the sample, to check for thermal gradients. None were observed within the experimental sensitivity, so this procedure was later simplified and only one thermometer was used. The total radioactive heating for the ^{46}Sc , ^{48}V , and ^{60}Co samples, which all emit energetic electrons that are largely absorbed in the sample, was about 7.5 nW; the ^{51}Cr and ^{54}Mn samples (electron capture decays) had less than 0.5 nW self-heating.

The samples were mounted by screwing the oxygen-free high-conductivity Cu holders into the coldfinger of a cerium magnesium nitrate adiabatic demagnetization cryostat. Construction details of this cryostat are given elsewhere;³⁰ a schematic diagram of the low-temperature parts and the sample holder is shown in Fig. 1. The cryostat could cool thin metal foils to below 3 mK, but in the present work, due to the unfavorable thermal properties of the samples as mentioned above, the minimum temperatures were near 6 mK. γ -ray spectra parallel to the applied magnetic field (and in some cases perpendicular to the field) were recorded using large-volume coaxial Ge(Li) detectors with a typical source-detector distance of 12 cm. In a usual demagnetization cycle, "warm" spectra were first recorded at the temperature of the pumped He precooling bath (about 1 K) with the compensated sample magnetizing coil at a particular field value. The demagnetization, lasting about 2 h, was then carried out, and cold spectra were recorded for some 20 h, during which time the sample gradually warmed to about 20 mK. Thereafter, He exchange gas was admitted to warm the sample to the precooler temperature and a second set of normalization spectra was recorded, after which the magnetizing field was changed to a new value and the next cycle begun.

The areas of all γ -ray peaks of interest in the spectra were obtained by a fit program which assumed a Gaussian peak shape and linear background, and automatically corrected for any small gain shifts which occurred during the cycle. γ -ray anisotropies $W(\theta)$ were calculated by normalizing the "cold" counting rates for each γ ray of interest and direction θ to the corresponding "warm" counting rates, correcting for counting-system dead time,

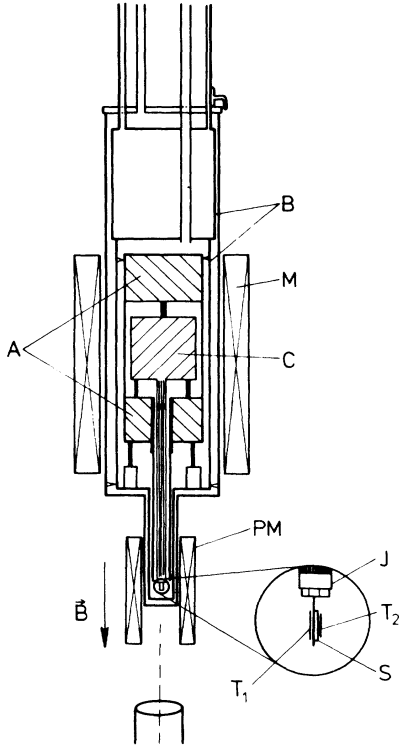


FIG. 1. Schematic of low-temperature apparatus. *B* is the 1-K bath and shield containing the paramagnetic salts *A* (iron alum, 25 mK shields) and *C* (cerium magnesium nitrate) which are magnetized by the 4.2-T coil *M*. The sample polarizing coil *PM* produces a field **B** of up to 7.5 T on the sample *S*, which is mounted together with two NO thermometers *T*₁ and *T*₂ on the threaded sample holder, *J*.

radioactive decay, and, where necessary, for the finite anisotropy at the temperature of the warm counts. The raw data for a given isotope thus consisted of a set of $W(\theta)$ values taken at various applied fields B ($1 \leq B \leq 7$ T) and temperatures ($6 \leq T \leq 25$ mK).

III. DATA ANALYSIS

As mentioned above, the electric quadrupole HFI is expected to be small for $3d$ impurities owing to the small quadrupole moments and antishielding factors. The large electric quadrupole HFI's reported in heavy rare earths³¹ are due to the unfilled $4f$ shells of the ions; while the open $3d$ shells of the transition elements may give rise to field gradients considerably larger than predicted by the point-charge model,¹⁹ these are still very small compared to the magnetic HFI (Ref. 22) and can be safely neglected in the analysis of the present experiments. Therefore, we have analyzed the data in terms of a magnetic HFI only. It was shown many years ago^{5,6} that the HFI of impurities in ferromagnetic hosts may be represented by an effective field B_{eff} acting at the impurity nuclei. (This may not be true for magnetic impurities in nonmagnetic host metals, where the HFI is the dominant interaction,³² nor with

techniques such as DPAC which are sensitive to the time evolution of the nuclear state.)

The γ -ray anisotropy of oriented nuclei is given by an expression of the form³³

$$W(\theta) = 1 + A_2 B_2 (\Delta/T) P_2(\cos\theta) + A_4 B_4 (\Delta/T) P_4(\cos\theta) + \dots, \quad (1)$$

where the A_k are known functions of the nuclear decay scheme and detection geometry, the P_k are Legendre polynomials, and the B_k are the moments of the nuclear orientation (diagonal elements of the statistical tensors $B_k^{(q)}$), which are functions of the hyperfine splitting Δ and the absolute temperature. The series on k terminates at $k \leq \min\{2I', 2L\}$, where I' is the smallest nuclear spin preceding the observed γ transition and L is the transition multipolarity. For all the isotopes studied here, $k \leq 4$ (and in the case of ^{160}Tb , where $E1$ transitions were observed, $k \leq 2$). Furthermore, only even values of k occur owing to parity conservation in γ decay. With a purely magnetic HFI described by an effective field, we have

$$\Delta = -\mu\mu_N B_{\text{eff}}. \quad (2)$$

In a nonsaturated ferromagnet, the local quantization axis is not necessarily parallel to the applied field **B**; thus, the angle θ in Eq. (1) is not well defined and an averaging procedure must be carried out to extract the B_k from a measurement of $W(\theta)$. It was shown in Ref. 24 for the case of Tb host that Eq. (1) is then modified as follows:

$$W(0^\circ) = 1 + A_2 \langle B_2 \rangle \langle P_2 \rangle + A_4 \langle B_4 \rangle \langle P_4 \rangle \quad (3)$$

and the effective field is now given by

$$\mathbf{B}_{\text{eff}} = \mathbf{B}_{\text{hf}} + (1 + K)(\mathbf{B} - \mathbf{B}_{\text{dm}}). \quad (4)$$

The coefficients $\langle P_k \rangle$ (denoted by ρ_k in Ref. 24) are averages of the corresponding Legendre polynomials over the angles α between the local quantization axis (direction of \mathbf{B}_{eff}) and the applied field **B**; 0° refers to detection of γ rays emitted parallel to **B** (Fig. 1.). \mathbf{B}_{eff} is the resultant of a vector addition of \mathbf{B}_{hf} (defined below) and **B**. Figure 2 illustrates the geometry implied by Eq. (4). The averages $\langle B_2 \rangle$ and $\langle B_4 \rangle$ take into account the variation of the magnitude of B_{eff} following Eq. (4), the average again being over angles α (Fig. 2). In Eq. (4), K is the Knight shift (which we assume to be less than 2% for transition impurities in Tb and therefore negligible in these experiments) and B_{dm} is the demagnetizing field of the sample (about 0.35 T for our disks at saturation).

In order to analyze the anisotropy data, the coefficients $\langle P_k \rangle$ in Eq. (3) must be determined. The basic procedure for doing this was described in Refs. 23, 24, and 26. Several variations are possible; the simplest, used in Ref. 23, is to treat $\langle P_2 \rangle$ and $\langle P_4 \rangle$ as unknown constants to be determined in the fit to the data, and to ignore the averaging over effective fields in the $\langle B_k \rangle$'s. The latter approximation is valid when the magnitude of B is small compared to that of B_{hf} , e.g., for MnTb (see below) or for TbTb , where the large orbital hyperfine field (> 300 T) is completely dominant, and $B_{\text{eff}} \cong B_{\text{hf}}$. The separation of the $k=2$ and $k=4$ terms may be accomplished by using

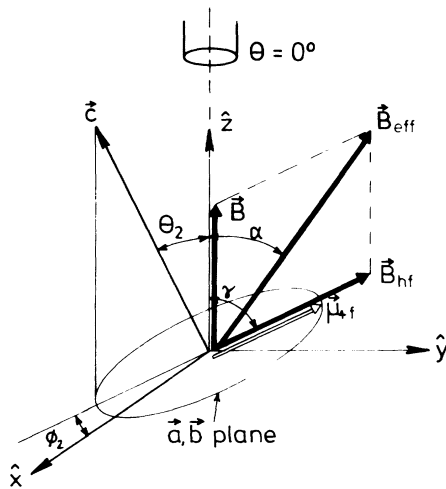


FIG. 2. Coordinate system for model calculations. The laboratory frame (x, y, z) is defined by the sample mounting geometry; a particular crystallite in the sample has its symmetry axes (a, b, c) oriented at angles θ_2 and ϕ_2 with respect to this frame. Due to crystalline anisotropy of the Tb host, the $4f$ moments remain in the basal plane but align as closely to \mathbf{B} as possible; the impurity hyperfine field \mathbf{B}_{hf} is assumed to be collinear with μ_{4f} and makes an angle γ with \mathbf{B} . The impurity quantization axis is the resultant field \mathbf{B}_{eff} , the vector sum of \mathbf{B}_{hf} and \mathbf{B} , which makes an angle α with \mathbf{B} . A detector at $\theta = 0^\circ$ is shown.

the rather different temperature dependence of B_2 and B_4 . If the $W(\theta)$ are first analyzed in terms of a fictitious “zero-order effective field” $B_{\text{eff}}^{(0)}$ by applying Eqs. (2) and (3), this quantity can be plotted against $1/T$ using various trial values of $\langle P_2 \rangle$ and $\langle P_4 \rangle$ until a temperature-independent $B_{\text{eff}}^{(0)}$ is obtained; a plot of the latter versus B then yields an approximate value for B_{hf} . See Ref. 23 for an example.

A more precise and generally applicable approach is to determine separately the averaged functions $\langle P_k \rangle$ and $\langle B_k \rangle$, either by means of a suitable computational model taking into account the magnetic structure of the host metal, or by supplemental experiments. The basic assumption used is that the local symmetry axis for a transition impurity will be determined by the local magnetization of the surrounding host material. This seems to be well fulfilled at low temperatures and high applied fields for the $3d$ impurities in Tb treated here. However, caution is advisable in applying this assumption generally, as strong deviations of the HFI of $4d$ and $5d$ impurities from the Tb host magnetization have been reported at higher temperatures (see Ref. 19 and references therein), and we have observed dramatic departures of impurity NO from the host magnetization in experiments on MnEr even at low temperatures.²⁶

Computations of $\langle P_2 \rangle$ for polycrystalline Tb and Dy hosts as a function of applied field were reported in Refs. 18 and 24, based on the known magnetic anisotropy constants of these metals. The main drawback to the exclusive use of such calculated magnetization distributions

is the possible presence of nonrandom crystallite orientations in the samples; therefore, an experimental check is desirable. This is provided by including ^{160}Tb activity in all of the samples and simultaneously determining the anisotropies of several of its γ rays as functions of B and T . Both the nuclear³⁴ and hyperfine²⁵ parameters are well known in this case, and only the $k=2$ term occurs in Eq. (3), as mentioned above; thus, the only unknown is $\langle P_2 \rangle$, which can be determined precisely for each value of B . Indeed, we find considerable preferential orientation of the crystallites in our pressed-disk samples, with the hexagonal a - b (basal) plane more likely to be in the sample plane. This makes the samples appear magnetically softer than predicted by a random-orientation calculation. Furthermore, this effect is found to be remarkably reproducible among a number of different samples, and to be similar to that reported by Krane³⁴ for arc-melted polycrystalline Tb. Only a spherical as-melted sample showed a rather different dependence of $\langle P_2 \rangle$ on B . These results were discussed in Ref. 24, where it was shown that a Gaussian weighting function for the crystallite orientation, included in the magnetization distribution calculation, gives a reasonable fit to the $\langle P_2 \rangle$ data from our samples. This function was used in subsequent model calculations.

The procedure adopted here to analyze all the anisotropy data for $3d$ impurities was as follows: “First-order effective field” values were determined from the anisotropies by inserting calculated $\langle P_2 \rangle$ and $\langle P_4 \rangle$ values, the former adjusted to give the best fit to the ^{160}Tb data, into Eq. (3) and solving for Δ/T , then combining with the measured temperatures to give $B_{\text{eff}}^{(1)}$ [Eq. (2)]. This quantity represents an average value due to the vector sum with \mathbf{B} at varying angles [Eq. (4)]. When plotted against B , it shows a nearly linear dependence, as might be expected from (4). Extrapolation to $B=0$ gives a rough value for B_{hf} , and the corresponding values for CrTb and MnTb were reported in Ref. 26. A more precise result is found by comparing the data points with a model calculation and varying the input value of B_{hf} to obtain best agreement; the actual dependence of $B_{\text{eff}}^{(1)}$ on B is complex, showing curvature depending on the magnitude of B_{hf} . Once B_{hf} has been determined in this way, a consistency check can be performed by calculating $W(\theta, B, T)$ directly and comparing with the observed γ -ray anisotropies. (One could use this approach from the beginning, but the intermediate analysis in terms of $B_{\text{eff}}^{(1)}$ yields an intuitively understandable result and allows an initial estimate of B_{hf} . We have previously applied a similar procedure, using a rather different model for the local symmetry axis distribution, to treat NO results from $^{60}\text{CoAuCo}$ alloys.³⁵)

IV. RESULTS AND DISCUSSION

A. Results

1. CoTb

The isotope ^{60}Co used here is standard in NO experiments and its nuclear parameters are well known (Table I). The ionic volume of Co^{3+} is considerably smaller than that of the Tb host, as is true of all the impurities studied

TABLE I. Nuclear properties of the isotopes studied. (Numbers in parentheses indicate reported errors in μ).

Isotope	Half-life ^a	γ-ray energy (keV)		A_2, A_4^b		I^a	$\mu (\mu_N)^a$
⁴⁶ Sc	83.8 d	889, 1120	-0.3651, -0.1307	4	3.03(2)		
⁴⁸ V	16 d	983, 1312	-0.3654, -0.1308	4	2.012(11) ^c		
⁵¹ Cr	27.7 d	320	0.556, 0.0137	$\frac{7}{2}$	0.934(5)		
⁵⁴ Mn	312 d	835	-0.4856, -0.4171	3	3.282(2)		
⁶⁰ Co	5.27 yr	1173, 1332	-0.4132, -0.2270	5	3.799(8)		
¹⁶⁰ Tb	72.1 d	299, 1272	-0.3396, -0.0038	3	1.702(8)		

^aFrom Ref. 36.

^bIncluding solid angle corrections for the higher energy gamma ray.

^cFrom Ref. 13.

here. Figure 3 shows the results obtained in terms of $B_{\text{eff}}^{(1)}$, with a linear approximation and the best-fit model calculations using $B_{\text{hf}} = -2.3$ T. [We have assumed a negative hyperfine field in plotting Fig. 3; this was verified by model calculations of the temperature dependence of $W(\theta)$.] Note the curvature of the model calculation, which gives a somewhat better fit than the linear approximation and is due to the vector addition of \mathbf{B} and \mathbf{B}_{hf} . The calculated field dependence of the anisotropy is shown in Fig. 4, along with the data for an average temperature of 12 mK. The sensitivity to the weighting func-

tion for crystallite orientations is seen to be minimal, and a variation of the order 0.3 T in B_{hf} is easily detectable within the statistical accuracy of the data. The reversal of the calculated anisotropy for $B \cong B_{\text{hf}}$ is due to the fact that in this region, a majority of the local quantization axes are oriented at angles between 55° and 125° with respect to \mathbf{B} , giving negative values for $\langle P_2 \rangle$. Figure 5 illustrates the calculated temperature dependence of $W(0)$ for two values of B ; these curves are rather sensitive to the assumed sign of B_{hf} , as shown below for Cr impurities, and confirm the negative sign in this case. The final

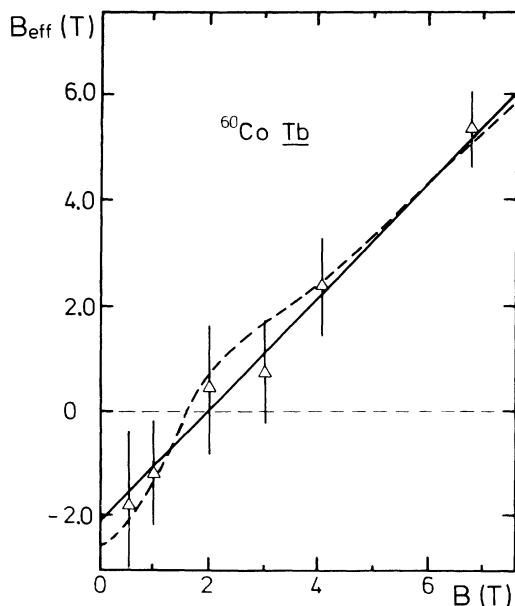


FIG. 3. First-order effective fields ($B_{\text{eff}}^{(1)}$, see text) determined for ⁶⁰Co in Tb (triangular points, statistical errors shown) as a function of applied field B . The solid line is a linear least-squares fit to the data points, and the dashed curve is the result of a model calculation for $B_{\text{hf}} = -2.3$ T (see text).

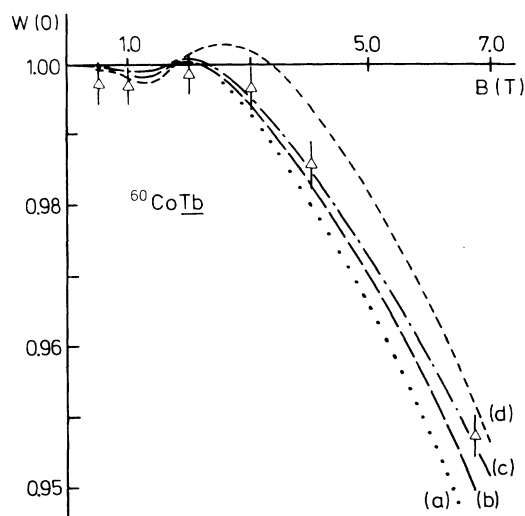


FIG. 4. Raw γ -ray anisotropy data (triangular points with statistical errors) for ⁶⁰Co in Tb versus B at approximately 12 mK. The curves are results of model calculations: (a) is for $B_{\text{hf}} = -2.0$ T and random crystallite orientation in the sample; (b) is the same hyperfine-field value but a Gaussian crystallite distribution with basal planes preferentially in the sample plane (Ref. 24); (c) is for $B_{\text{hf}} = -2.3$ T, and (d) for -3.0 T. Note the anisotropy reversal in the calculated curves near $B \cong B_{\text{hf}}$.

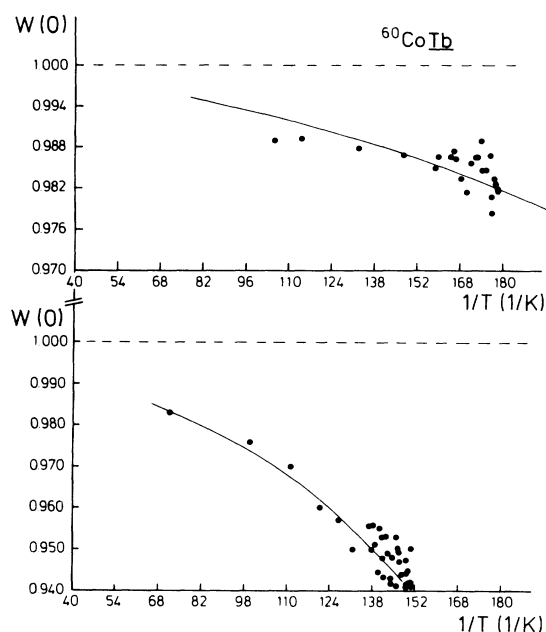


FIG. 5. γ -ray anisotropies from ^{60}Co in Tb at $B = 4$ T (upper part) and $B = 6.7$ T (lower part), as a function of inverse sample temperature. The data points are shown without errors, and the curves are results of a model calculation for $B_{\text{hf}} = -2.3$ T.

value for B_{hf} , corrected for the demagnetizing field (assuming 80% average saturation; see Ref. 24), is $-2.0(3)$ T.

2. MnTb and CrTb

The properties of the isotopes ^{54}Mn and ^{51}Cr are summarized in Table I. The latter is the least favorable isotope for NO used here, owing to its small nuclear moment. These impurities were present in the samples in concentrations of several ppb. Figure 6 shows the effective

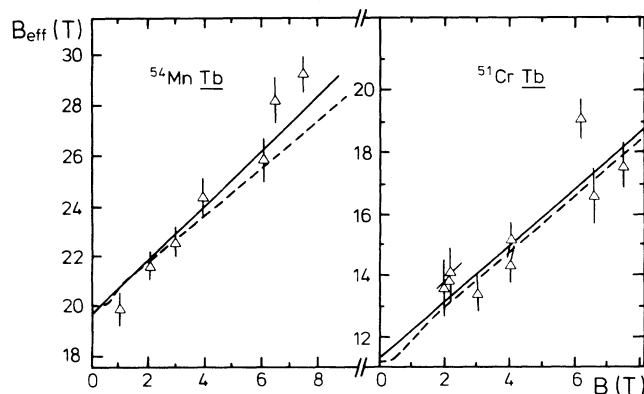


FIG. 6. $B_{\text{eff}}^{(1)}$ vs B for ^{54}Mn and ^{51}Cr impurities in Tb, similar to Fig. 3.

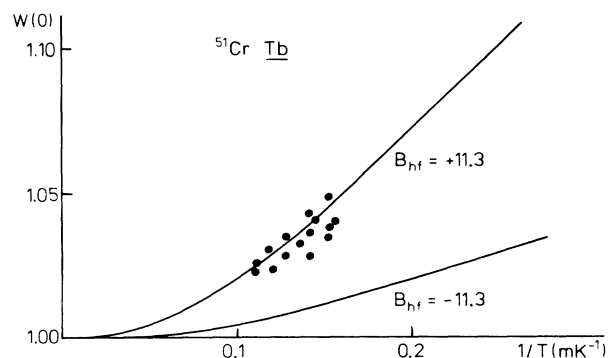


FIG. 7. γ -ray anisotropies measured for ^{51}Cr in Tb at $B = 3$ T, compared to model calculations for B_{hf} of magnitude 11.3 T and either sign. The positive sign is clearly correct.

field plots for these two systems. The observed fields are large and positive in both cases; the curvature of the calculated dependence is reduced here compared to CoTb, due to the larger magnitudes of B_{hf} . The positive sign was confirmed by fits to the temperature dependence of the γ -ray anisotropy like those displayed in Fig. 7, where the drastic difference from the curves calculated for a negative field is clear. The values of B_{hf} , corrected for demagnetizing field, are MnTb, $+20.0(1.0)$ T and CrTb, $+11.6(1.0)$ T. (These differ somewhat from the preliminary results reported in Refs. 23 and 26 due to the more elaborate analysis procedure used here, and supercede the latter values.)

3. VTb and ScTb

The isotopes used have well-known, favorable nuclear properties. The valence shell of Sc is isoelectronic with that of Tb and the two metals form a wide range of solid solutions, in contrast to the other impurities studied. However, the ionic volume of Sc is still less than $\frac{2}{3}$ of that of Tb. Trivalent Sc has the [Ar] configuration and is thus not expected to develop a local moment. Figure 8 again shows data and calculations for the effective fields, which are found to be negative and relatively small. A strong anisotropy reversal, similar to that seen in Fig. 4 for $B \cong B_{\text{hf}}$, is observed in both cases (see Fig. 9); the data points in this field range have therefore been omitted. This reversal was in both cases stronger than predicted by the model calculations, although the fit at higher values of B was good. Systematic variation of the assumed crystalline anisotropy constants and crystallite distributions failed to reproduce the observed large reversed-anisotropy values, which indicate a local disalignment of the Sc and V hyperfine fields from the surrounding $4f$ moments. Such effects are well known in amorphous rare-earth- $3d$ intermetallic compounds,³⁷ where the $4f$ moments follow the lattice crystalline anisotropy axes while the $3d$ moments order ferromagnetically or antiferromagnetically. They are rather unexpected in crystalline materials, however, although we have observed similar, but even more

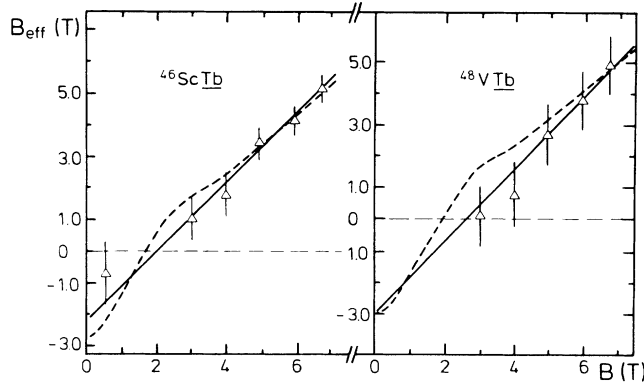


FIG. 8. First-order effective fields versus applied field as in Figs. 3 and 6, for ^{46}Sc and ^{48}V impurities in Tb.

drastic disalignment effects in MnEr at intermediate fields, as mentioned above. The deviations have little effect on the derived values for B_{hf} , which are mainly determined by the high-field points. The corrected values are VTb , $-2.4(5)$ T and ScTb , $-2.0(4)$ T. The negative signs were again confirmed by comparison with the calculated temperature dependences of $W(0)$.

B. Discussion

The hyperfine fields determined above are sums of several different contributions, which must be separated

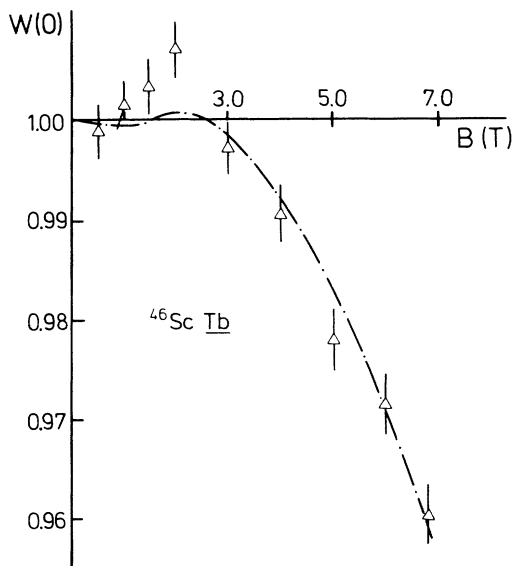


FIG. 9. The field dependence of the γ -ray anisotropy from ^{46}Sc in Tb near 12 mK, along with a model calculation curve for $B_{\text{hf}} = -2.3$ T. Note the large anisotropy reversal observed around $B = 2$ T, indicating local misalignment between the host magnetization (as represented by the calculated curve) and the impurities' quantization axes (data points).

to allow further interpretation. We may write

$$B_{\text{hf}} = B_{\text{int}} + B_{\text{host}}, \quad (5)$$

with

$$B_{\text{int}} = B_{\text{loc}} + B_{\text{tr}} \quad \text{and} \quad B_{\text{host}} = B_{\text{Lor}} + B_{\text{HD}}.$$

The field B_{host} is simply the field at the impurity nucleus due to the magnetization of the surrounding host material, and contains the Lorentz field, B_{Lor} , as well as the host-dipole field, B_{HD} , due to host moments inside the Lorentz sphere. We estimate B_{host} to be $+1.15$ T for Gd and $+1.35$ T for Tb. This contribution is subtracted from the measured B_{hf} to give B_{int} , the "internal" field at the impurity nuclei due to electrons from the impurity ion and the host. This field can be further decomposed into local and transferred contributions, as indicated above. The values of B_{int} which are known for transition impurities in Tb are set out in Table II, column 3, along with corresponding fields in Gd host, for comparison (column 2).

To continue the decomposition of the hyperfine fields, we must consider the contributions to B_{loc} and B_{tr} . The latter is due to the host conduction-electron polarization (CEP) and to volume-overlap effects:

$$B_{\text{tr}} = B_{\text{CE}} + B_{\text{vol}}. \quad (6)$$

Owing to the small impurity ionic volumes mentioned above, we can assume the volume-overlap field B_{vol} to be zero. The only remaining volume-mismatch effects produce a renormalization of the conduction-electron field, B_{CE} , which will be automatically taken into account in estimating the latter.

The usual procedure for estimating B_{CE} , if no calculated values are available, is to obtain the hf fields at non-magnetic impurities at the beginning and end of the impurity transition series in the given host, attribute them to B_{CE} , and interpolate through the series. This procedure ignores local environment effects (LEE), i.e., changes in the host moments near an impurity site which lead indirectly to changes in B_{CE} ; also, the precise form of the interpolation is open to question. Neglect of LEE should not be a serious problem in the heavy RE hosts, where the host moments are mainly due to well-localized $4f$ electrons and are essentially atomiclike.

When the fields at impurities from the ends of a particular transition series are unknown, they can be estimated by comparison with those at other (preferably isoelectronic) impurities or in other hosts.²⁰ A rough approximation is to scale by the ratio of host magnetizations (or that portion of the magnetization attributable to CEP). This neglects possible impurity-dependent renormalization effects as discussed below.

From Table II, we see that fields at Au and Hf as well as Sc impurities in Tb are now known. The ratio of "excess magnetizations" in Tb and Gd hosts (over that due to atomic $4f$ moments) is 0.56, in good agreement with the ratios of B_{int} for $\text{ScTb}:\text{ScGd}$, 0.61(16) and for $\text{AuTb}:\text{AuGd}$, 0.54(2). The Hf field ratio is 1.0(2), in seri-

TABLE II. Summary of hyperfine data for Gd and Tb hosts. (Numbers in parentheses indicate statistical errors.)

Impurity	$B_{\text{int}}(\text{Gd})^a$	$B_{\text{int}}(\text{Tb})$	B_{CE}^b	B_{loc}	$R_S(T/\mu_B)^c$	$\mu_S (\mu_B)$
Sc	-5.50(65)	-3.35(40) ^d	-3.20	-0.15(40)	-5.5	+0.03(7)
(Ti)	-10.15(50)	-4.0(9) ^e	-3.24	-0.76(90)	-6.0	+0.13(16)
V	-9.90(90)	-3.75(50) ^d	-3.54	-0.21(50)	-6.5	+0.03(8)
Cr	+1.20(55)	+10.3(1.0) ^d	-3.88	+14.2(1.0)	-7.0	-2.02(15)
Mn	+17.50(45)	+18.7(1.0) ^d	-4.22	+22.9(1.0)	-7.5	-3.06(13)
Fe	+1.85(30) ^f	+1.20(20) ^f	-4.56	+5.76(20)	-8.0	-0.72(3)
Co	-5.40(40)	-3.35(30) ^d	-4.88	+1.53(30)	-8.5 [-6.0]	-0.18(4) [-0.25]
(Ni)	-8.35(50)	-4.80(60) ^e	-5.14	+0.34(60)	-8.5 [-5.0]	-0.04(7) [-0.07]
(Cu)	-10.15(50)	-5.66(35) ^g	-5.34	-0.32(35)		
Hf	-38.6(3.5)	-39.4(5.0) ^h				
Au	-82.05(80)	-44.0(1.3) ⁱ				

^aFrom Ref. 17.

^bEstimated as described in text.

^cFrom Ref. 2; see text for explanation of values in square brackets.

^dPresent work.

^eEstimated from systematics (Fig. 11).

^fFrom Ref. 19.

^gEstimated from fields at AuTb and AuGd.

^hFrom Ref. 38.

ⁱFrom Ref. 39.

ous disagreement, and the reported field at HfTb is probably in error, given its general deviation from systematics. These ratios were used to estimate B_{int} for CuTb, giving an average value of $-5.66(35)$ T. In contrast, the ratio of $4f$ spin moments for Tb:Gd is 0.86, indicating either that considerable renormalization of the spin-polarization field occurs between the two hosts, or that orbital contributions are important. We consider the origin of B_{CE} in more detail to clarify this question.

In an alloy where orbital magnetism of the conduction electrons is important, B_{CE} may be described by four terms:⁴⁰

$$B_{\text{CE}} = B_d + B_s + B_{10} + B_{21} . \quad (7)$$

The first two terms are due to spin polarization and are proportional to the host spin moments, $(g_J - 1)\langle J_z \rangle$, where g_J is the host Landé g factor and $\langle J_z \rangle$ the average angular momentum (usually taken to have its maximum value, $\langle J_z \rangle = J$). The first term is due to polarization of the inner s electrons of the impurity ion by interaction with spin-polarized d -like conduction electrons, and is proportional to R_{CP} , the core-polarization hyperfine-field constant, which has been calculated by Freeman and Watson.⁴¹ The second term is the direct contact field arising from polarized s -like conduction electrons with a finite density at the impurity nucleus; calculations of the corresponding hyperfine-field constant $A(Z)$ have been performed by Campbell³ and by Watson and Bennett.⁴² For $3d$ impurities, $A(Z)$ is typically more than an order of magnitude larger than R_{CP} , while we may expect the d -electron spin moment at an impurity site in Tb to be about 3 times larger than that of the s electrons (from a recent band-structure calculation⁴³ for Gd). These two

contributions may thus be combined using an effective value of $A(Z)$.

The last two terms in Eq. (7) are due to orbital and spin-dipolar conduction-electron interactions, respectively, and are proportional to the corresponding host moments, $(2 - g_J)\langle J_z \rangle$ and $c_n \langle J_z \rangle$, with c_n a matrix element calculated in Ref. 40. Taking $\langle J_z \rangle = J = 6$, $g_J = \frac{3}{2}$, and $c_n = -\frac{1}{12}$ for Tb, we can simplify Eq. (7):

$$B_{\text{CE}}(\text{Tb host}) = 3H_{01}[1 + b_{10} - b_{21}/6] , \quad (8)$$

where H_{01} is a coefficient proportional to the spin-polarization fields (B_s and B_d as defined above) and the $b_{1,1'}$'s are ratios of the corresponding coefficients for the orbital and spin-dipolar contributions: $b_{10} = H_{10}/H_{01}$ and $b_{21} = H_{21}/H_{01}$.

Equation (7) was originally proposed to explain deviations from proportionality to $(g_J - 1)J$ of hf fields at nonmagnetic impurities along the series of RE hosts.⁴⁰ Other explanations which have been suggested are a variation of the exchange coupling constants J_{01} due to interband mixing effects,⁴⁴ and deviations⁴⁵ from $\langle J_z \rangle = J$. In the absence of orbital terms, these effects would simply renormalize B_{CE} in a given host and would be automatically included in the hf field ratios quoted above. Dunlap *et al.*⁴⁰ also point out that where spin-orbit effects are important for the conduction electrons, as might be expected for heavy RE hosts, the ratios $b_{1,1'}$ are simply given by the ratios of the corresponding coupling constants, $J_{1,1'}/J_{01}$. They are thus essentially host properties, and also lead only to an effective renormalization of B_{CE} for a series of transition impurities in a given host.

However, a comparison of fitted constants H_{01} , b_{10} , and b_{21} for several nonmagnetic impurities³⁹ has shown a

strong impurity dependence. Berthier *et al.*⁴⁵ studied RE dialuminides and found, paradoxically, that orbital terms were necessary to explain the observed B_{CE} values at RE sites, but not those on the Al sites. To estimate the relative importance of the b_{10} and b_{21} terms in Eq. (8), we have assumed them to be proportional to calculated spin-orbit splitting constants λ or to $\langle r^{-3} \rangle$, and have used ratios of $\lambda/A(Z)$ or $\langle r^{-3} \rangle/A(Z)$ to scale the fitted constants for Hf and Au to the 3d-series impurities. The results of these various estimation procedures are summarized in Fig. 10.

Curve (a) of Fig. 10 represents a simple scaling of B_{CE} for Sc and Cu in Gd host by the host CE-magnetization ratio, with linear interpolation. Curve (b) is an extrapolation from ScTb using the calculated $A(Z)$'s of Ref. 42, and gives an unrealistically large magnitude for the field at CuTb [the $A(Z)$ values of Ref. 3 yield an even steeper slope and are not shown]. Curve (c) is the result of re-scaling fitted constants³⁹ for Au using $\lambda/A(Z)$ (Ref. 3), while curve (e) is a similar rescaling using $A(Z)$ from Ref. 42 and additionally normalizing to the measured ScTb field. Curve (d) represents a rescaling of the Hf fit constants by $\langle r^{-3} \rangle/A(Z)$ (Refs. 41 and 42), and curve (f) is the same curve normalized to the ScTb field.

In the absence of clear information about the impurity dependence of B_{CE} , we have taken averages of curves (a), (d), and (e) in Fig. 10 to represent a reasonable estimate (Table II, column 4). This gives the smooth dot-dashed curve shown in Fig. 11, with estimated uncertainties of ± 0.4 T near Sc, increasing to ± 0.6 T near Cu, i.e., comparable to the uncertainties in the measured B_{int} values.

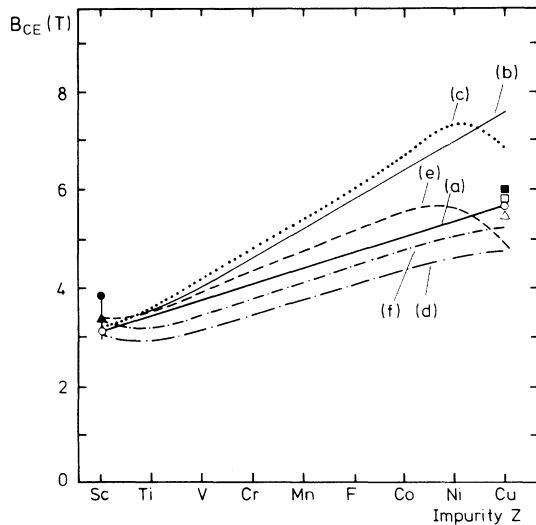


FIG. 10. Estimates of the CEP contribution to the internal field at 3d impurities in Tb. The solid triangle with error bars is the value for ScTb from the present work; the open circles show estimated fields at Sc and Cu using the CE-magnetization ratio and known fields in the Gd host. The solid circle is calculated for Sc using the reported field on Hf and the $A(Z)$'s of Ref. 3; the open triangle is calculated for Cu from the field ratio for Au impurities in Tb and Gd, and the square points are estimated from the field at AuTb with the $A(z)$'s of Refs. 3 and 42. The curves are the results of various interpolation procedures and are explained in the text.

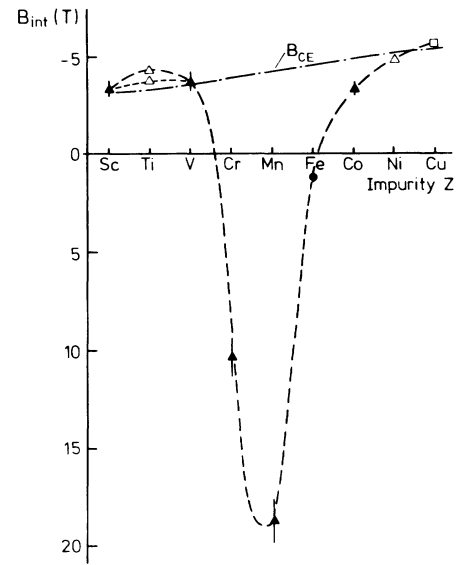


FIG. 11. Systematics of the internal fields at 3d-series impurities in Tb. The solid triangles are from the present work, the solid circle from Ref. 19. The open square for Cu is the field estimated from that on Au. The dashed curve indicates the systematic trend and the open triangles are interpolated fields for Ti (two possible interpolations) and Ni impurities. The dot-dashed curve shows the estimated CEP contributions to B_{int} (see Fig. 10 and Table II).

The latter are also shown in the figure, connected by a dashed curve to indicate the systematic trend and to illustrate the estimation of B_{int} for TiTb and NiTb. The values of B_{loc} , obtained by subtracting B_{CE} from B_{int} , are given in Table II, column 5.

The local field, B_{loc} , can be decomposed as follows:

$$B_{loc} = B_{CP} + B_{SP} + B_{orb} + B_{SD}, \quad (9)$$

where we have ignored the (small) second-order spin-dipolar contribution.⁵ Equation (9) strongly resembles Eq. (7), and contains the corresponding local-field contributions. The first two terms are due to the formation of an impurity spin moment μ_S , and are given by $B_{CP} = R_{CP}\mu_S$ (core-polarization field) and $B_{SP} = A(Z)p_S\mu_S$ (self-polarization field), respectively. Here, R_{CP} and $A(Z)$ are the hyperfine-field constants defined above, and p_S is the local polarization (in s -electron spins) produced by a spin moment of one μ_B . These two terms can be combined into a "local spin field" B_S , and we may write

$$B_S = (B_{CP} + B_{SP}) = [R_{CP} + A(Z)p_S]\mu_S = R_S\mu_S. \quad (10)$$

The last equation defines an effective spin hyperfine-field constant R_S . Since B_{CP} is negative and B_{SP} is positive, the two contributions partially cancel and R_S is reduced compared to R_{CP} as calculated for a pure 3dⁿ configuration. It is not possible to separate the two terms experimentally, but comparison of hyperfine fields with local moments determined by $d\mu/dc$ or neutron scattering

measurements can be used to estimate R_S . The values shown in Table II, column 6, were obtained by uniformly reducing the calculated R_{CP} 's from Ref. 41 and give reasonable agreement with the moments in Fe host;²⁻⁴ a more-detailed comparison is made in Ref. 46. If the restriction of a uniform reduction of the calculated constants is relaxed, even better agreement with the Co and Ni moments is obtained using the values in square brackets, which are more strongly reduced. This tendency for B_{loc} to be more positive for impurities near the end of the transition series has been observed in many host environments^{35,47-49} and has been attributed both to orbital fields, which are positive, and to the predominance of B_{SP} over B_{CP} ; in some cases, R_S itself has been reported to become positive at the end of the 3d series,⁴⁹ and this has been ascribed to a strong increase in B_{SP} .

The last two terms in Eq. (9) are the orbital field ($B_{orb} = R_{orb}\mu_{orb}$) and the spin dipolar field. Both should increase as $\langle r^{-3} \rangle$ and thus towards the end of the transition series, and are small or vanishing in cubic symmetry. These fields are both positive, so that neglecting them in evaluating B_S would lead us to overly positive values; this, in turn, would cause the spin moments derived using Eq. (10) to be overestimated if they are negative and to be underestimated if they are positive, i.e., the spin-moment systematics curve (Fig. 12) would be shifted downwards, more strongly for impurities of higher Z . An estimate of the importance of these effects may be obtained by comparing the moment systematics for hexagonal Co host with those for cubic Ni. Orbital and spin-dipolar fields should be present in the former host, especially for Co and

Ni, possibly for Fe impurities, but absent in the latter. The curve for Co host is, in fact, shifted to more negative values compared to that in Ni, although the difference for Ni impurities is insignificant; the shift amounts to roughly $1\mu_B$ for Fe and Co and $0.5\mu_B$ for V, but vanishes for Mn impurities (and probably for Cr, whose hyperfine field in the Co host is unknown). This gives an estimate of the effect of neglecting the orbital and spin-dipolar fields in Eq. (9). (We note that the local fields observed in the Tb host are all positive within the quoted errors, so that they could, in principle, be explained as being due *only* to $B_{orb} + B_{SD}$; this assumption contradicts all that is known about local moment formation and would result in a rather bizarre dependence of the orbital moments on impurity Z , so we have not considered it seriously.) We shall discuss the interpretation of Fig. 12 in more detail in the concluding section.

V. CONCLUSIONS

The localized (spin) moments in the Tb host obtained in a straightforward way using Eqs. (9) and (10) with the R_S values from Table II, and neglecting orbital and spin-dipolar fields, are listed in the last column of Table II for the Tb host and are plotted in Fig. 12, where they are compared with similarly-derived values for Co, Ni, and Gd hosts. The curves all have the same structure: a weak maximum in the first half of the series, a zero crossing near the middle, and a strong maximum of opposite sign in the second half of the series. The general trend can be understood in terms of increasing d -electron localization⁴ with increasing impurity Z and of the coupling of the local moments to the host conduction band.⁵⁰ As we have seen, the curves for Co and Ni hosts are very similar, except for small effects which may be due to the neglect of orbital contributions to B_{loc} in the former. Turning to a comparison of the RE hosts Gd and Tb, we see that the moments for a given 3d impurity are the same within combined errors, with the exceptions of Cr and Fe; in particular, the large Mn moments are practically identical. A small but systematic trend to more positive moments on impurities above Mn and more negative values on impurities below Mn in the Tb host is observed, which makes the systematics curve for Tb appear to be shifted slightly to lower Z relative to that for Gd. However, the differences are minimal, and we conclude that the strong orbital magnetism of Tb, which makes the host properties very different from those of Gd, have essentially no influence on impurity moment formation.

Comparing the moments in RE hosts with those in elemental 3d ferromagnets, we note two striking differences: the sign of the moments is reversed in the two types of host, and the systematics curves are shifted as a whole to lower Z values in the RE hosts. These differences persist in the 4d and 5d impurity series (where the magnitudes of the moments are, however, considerably smaller).^{20,21,51} In Refs. 3, 20, and 21, it was suggested that the sign reversal could be understood simply in terms of Moriya's rule for local moment formation in transition-metal hosts,⁵⁰ if the heavy RE (in particular Gd) were considered to have important d - f interactions and d -electron

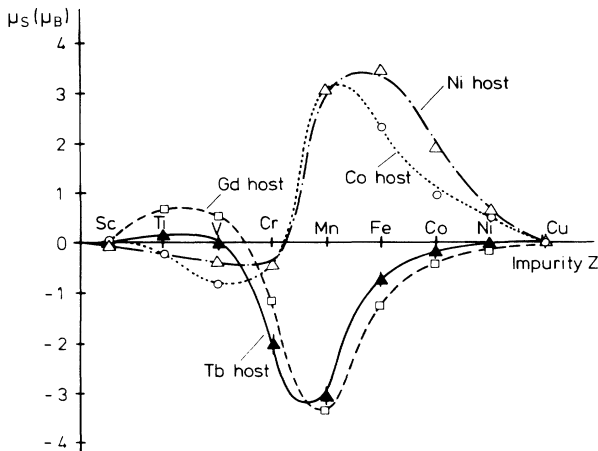


FIG. 12. Derived spin moments on 3d impurities in the 3d ferromagnetic hosts Co and Ni and the heavy RE hosts Gd and Tb. The moments were derived using the procedure outlined in the text and hyperfine fields from Ref. 17 (Co, Ni, and Gd hosts) and the present work (Tb host), and the R_S values from Table II, column 6. The errors shown for the Tb host are from the statistical errors in B_{int} only; those for the other hosts are comparable. Additional systematic errors are probably smooth functions of impurity Z and would not drastically change the shape of the curves or the comparison among the different hosts.

polarization, in contrast to the assumptions of the classical s - f model. In this picture, Gd (or other heavy RE hosts) behaves as a transition metal at the beginning of the series when viewed from an impurity site; Moriya's rule then predicts positive local moments for impurities from the first half on an nd series and negative moments in the second half. The importance of d -electron polarization in Gd has been borne out by band-structure calculations.^{43,52}

Recently, this interpretation of the hyperfine data in the Gd host has been called into question by Leal *et al.*,⁵¹ who propose an extended Ruderman-Kittel-Kasuya-Yoshida model and have calculated B_S and B_{CE} for $5d$ -series impurities in Gd. As they point out, Moriya's rule was obtained for paramagnetic hosts and is thus not necessarily applicable to ferromagnets; however, it works rather well for the $3d$ elemental ferromagnets (Fig. 12) as well as for $3d$ -based ferromagnetic intermetallic compounds.^{46,49} We note that while the calculated fields of Ref. 51 agree with the general trend of the experimental values, there are considerable deviations for some impurities, particularly for Hf, Ta, and Os. If the moments are derived from the hyperfine data as described above, a significant positive moment is found for Hf, and the principal maximum of the moment curve occurs at Os; the shape is rather similar to that found for $3d$ impurities in this work, except that the (negative) moments on Re, Os, and Ir are relatively larger in magnitude. This is just what would be expected due to neglect of orbital and spin-dipolar fields, which may be important in the $5d$

series. Allowing for this possibility, the spin-moment curves in Gd host are rather similar in the $3d$ and $5d$ impurity series, and the latter again represent a mirror image of the corresponding curve for Ni host, except that the maxima are shifted to lower impurity Z . It is thus probably premature to conclude that an interpretation based on Moriya's model is not correct. The origin of the systematic shifts of the moment curves in RE hosts compared to $3d$ hosts is not clear, but it may well be related to changes in local electron concentrations at the impurity sites due to the differing electronegativities of transition elements and rare earths.

In summary, we have measured hyperfine fields at most of the $3d$ transition metals as impurities in ferromagnetic Tb. Combining the results with other work and with interpolations from systematics, we can estimate the local moments formed on these impurities and find them to be quite similar to those derived for Gd host. The results are consistent with a d - d coupling model proposed earlier.

ACKNOWLEDGMENTS

We thank Dr. I. A. Campbell for useful discussions, and Mr. G. Muschert for technical assistance. The work was supported in part by the Deutsche Forschungsgemeinschaft (Sonderforschungsbereich 161) and forms a part of the dissertation of J.B. Our ^{160}Tb irradiations were performed at the BER II Reactor, Hahn-Meitner-Institut, Berlin.

*Present address: Bundesanstalt für Materialprüfung, D-1000 Berlin 45, Germany.

¹D. A. Shirley and D. A. Westenbarger, Phys. Rev. **138**, A170 (1965).

²D. A. Shirley, S. S. Rosenblum, and E. Matthias, Phys. Rev. **170**, 363 (1968).

³I. A. Campbell, J. Phys. C **2**, 1338 (1969).

⁴M. B. Stearns, Phys. Rev. B **13**, 1183 (1976).

⁵W. Marshall, Phys. Rev. **110**, 1280 (1958); D. A. Goodings and V. Heine, Phys. Rev. Lett. **5**, 370 (1960).

⁶R. E. Watson and A. J. Freeman, Phys. Rev. **123**, 2027 (1961).

⁷P. Léonard and N. Stefanou, J. Phys. (Paris) **43**, 1497 (1982).

⁸S. Shinozaki and A. Arrot, *Proceedings of the IX International Conference on Low Temperature Physics, Columbus, 1964*, edited by J. G. Daunt, D. O. Edwards, F. J. Milford, and M. Yaqub (Plenum, New York, 1965), p. 1066.

⁹M. Kontani, T. Hioki, and Y. Masuda, J. Phys. Soc. Jpn. **32**, 416 (1972); Y. Masuda, T. Hioki, and M. Kontani, Int. J. Magn. **6**, 143 (1974).

¹⁰T. J. Burch, J. I. Budnick, V. A. Nicolescu, K. Raj, and T. Li-trenta, Phys. Rev. B **24**, 3866 (1981).

¹¹S. S. Hanna, J. Haberle, C. Littlejohn, G. J. Perlow, R. S. Preston, and D. H. Vincent, Phys. Rev. Lett. **4**, 177 (1960); I. Vincze and I. A. Campbell, J. Phys. F **3**, 647 (1973).

¹²J. Soares, K. Krien, and K. Freitag, Hyperfine Interact. **1**, 45 (1975); K. Johannson, E. Karlsen, and L. O. Noerlin, J. Phys. F **8**, 337 (1978).

¹³K.-D. Bures, W. D. Brewer, and G. V. H. Wilson, Hyperfine Interact. **8**, 59 (1980); J. Boysen, A. Kettschau, and W. D.

Brewer, Phys. Lett. **95A**, 502 (1983).

¹⁴A. T. Aldred, Int. J. Magn. **2**, 223 (1973); F. Kajzar and G. Parette, J. Appl. Phys. **50**, 1966 (1979).

¹⁵M. F. Collins and G. G. Low, Proc. Phys. Soc. **86**, 535 (1965); M. B. Stearns and I. A. Feldkamp, Phys. Rev. B **13**, 1198 (1976).

¹⁶F. Kajzar and G. Parette, J. Magn. Magn. Mater. **14**, 253 (1979).

¹⁷G. N. Rao, Hyperfine Interact. **7**, 14 (1979).

¹⁸K. Kroth, W. Thomas, D. Mertin, and M. Forker, Hyperfine Interact. **2**, 206 (1976); K. Kroth, D. Mertin, W. Thomas, and M. Forker, Z. Phys. B **27**, 241 (1977).

¹⁹M. Forker, R. Trzcinski, and T. Merzhaeuser, Hyperfine Interact. **15/16**, 273 (1983).

²⁰I. A. Campbell, W. D. Brewer, J. Flouquet, A. Benoit, B. W. Marsden, and N. J. Stone, Solid State Commun. **15**, 711 (1974).

²¹W. D. Brewer and E. Wehmeier, Phys. Rev. B **12**, 4608 (1975).

²²W. D. Brewer, J. Phys. F **7**, 693 (1977).

²³J. Grimm, W. D. Brewer, and G. V. H. Wilson, J. Phys. (Paris) Colloq. **40**, C5-58 (1979).

²⁴J. Grimm, J. Boysen, W. D. Brewer, and G. V. H. Wilson, J. Phys. F **13**, 1931 (1983).

²⁵P. Roman, W. D. Brewer, E. Klein, H. Marshak, K. Freitag, and P. Herzog, Phys. Rev. Lett. **56**, 1976 (1986).

²⁶J. Grimm, W. D. Brewer, J. Boysen, and G. V. H. Wilson, Hyperfine Interact. **10**, 861 (1981).

²⁷K. Rasmus Co., Hamburg.

²⁸M. A. R. Leblanc and W. T. Sommer, *Proceedings of the VIII*

- International Conference on Low Temperature Physics, London, 1962*, edited by R. O. Davies (Butterworths, London, 1963), p. 432.
- ²⁹D. Oertel, A. Ketschau, and W. D. Brewer, *Z. Phys. A* **310**, 233 (1983); H. Ernst, E. Hagn, E. Zech, and G. Eska, *Phys. Rev. B* **19**, 4460 (1979).
- ³⁰W. D. Brewer and D. H. Chaplin, in *Low Temperature Nuclear Orientation*, edited by N. J. Stone and H. Postma (North-Holland, Amsterdam, 1986), Chap. 17.
- ³¹*Magnetic Properties of Rare Earth Metals*, edited by R. J. Elliot (Plenum, London, 1972), p. 383ff.
- ³²J. Flouquet, in *Progress in Low Temperature Physics*, edited by D. F. Brewer (North-Holland, Amsterdam, 1978), Vol. VIIB.
- ³³R. J. Blin-Stoyle and M. A. Grace, *Handbuch der Physik* **42**, 555 (1957).
- ³⁴K. S. Krane, *Nucl. Phys. A* **377**, 176 (1982).
- ³⁵J. Boysen, W. D. Brewer, and E. Klein, *Hyperfine Interact.* **1**, 55 (1974).
- ³⁶*Table of Isotopes*, 7th ed., edited by C. M. Lederer and V. S. Shirley (Wiley, New York, 1978).
- ³⁷J. M. D. Coey, J. Chappert, J. P. Rebouillat, and T. S. Wang, *Phys. Rev. Lett.* **36**, 1061 (1976).
- ³⁸S. G. Cohen, N. Kaplan, and S. Ofer, *Proceedings of the International Conference on Magnetism, Nottingham, 1964* (IOP, London, 1964), p. 233.
- ³⁹J. Perscheid and M. Forker, *Z. Phys. B* **31**, 49 (1978).
- ⁴⁰B. D. Dunlap, I. Nowik, and P. M. Levy, *Phys. B* **7**, 4232 (1973).
- ⁴¹A. J. Freeman and R. E. Watson, in *Magnetism*, edited by G. T. Rado and H. Suhl (Academic, New York, 1965), Vol. IIA, p. 167.
- ⁴²R. E. Watson and L. H. Bennett, *Phys. Rev. B* **15**, 502 (1977).
- ⁴³J. Sticht and J. Kuebler, *Solid State Commun.* **53**, 529 (1985).
- ⁴⁴R. E. Watson, A. J. Freeman, and S. Koide, *Phys. Rev.* **186**, 625 (1969).
- ⁴⁵Y. Berthier, R. A. B. Devine, and E. Belorizky, *Phys. Rev. B* **17**, 4137 (1978).
- ⁴⁶J. Boysen, A. Heidari, and W. D. Brewer, *J. Magn. Magn. Mater.* **59**, 15 (1986).
- ⁴⁷A. Narath and B. Barham, *Phys. Rev. B* **7**, 2195 (1973).
- ⁴⁸G. M. Kalvius, T. E. Katila, and O. V. Lounasmaa, *Mössbauer Effect Methodol.* **5**, 231 (1970); J. Flouquet, O. Taurian, J. Sanchez, M. Chapellier, and J. L. Tholence, *Phys. Rev. Lett.* **38**, 81 (1977); A. L. Erzinkyan, V. V. Murav'eva, V. P. Perfenova, and V. V. Turovtsev, *Zh. Eksp. Teor. Fiz.* **77**, 1087 (1979) [*Sov. Phys.—JETP* **50**, 548 (1979)].
- ⁴⁹V. A. Niculescu, T. J. Burch, and J. I. Budnick, *J. Magn. Magn. Mater.* **39**, 223 (1983).
- ⁵⁰T. Moriya, *Progr. Theor. Phys.* **34**, 329 (1965).
- ⁵¹C. E. Leal, O. L. T. de Menezes, and A. Troper, *Solid State Commun.* **53**, 35 (1985).
- ⁵²B. N. Harmon, *J. Phys. (Paris) Colloq.* **40**, C5-65 (1979).